AGU PUBLICATIONS

Paleoceanography

RESEARCH ARTICLE
10.1002/2015PA002914

Key Points:
- Inharmonious temperature changes between surface/thermocline waters in glacial-interglacial cycles
- Intermediate water contributes to thermocline warming in the North Pacific Subtropical Gyre
- Kuroshio Current and intermediate water largely affect North Pacific Subtropical Gyre evolution

Supporting Information:
- Supporting Information S1

Correspondence to:
Y. Ujiié,
yujiie@kochi-u.ac.jp

Citation:
Ujiié, Y., H. Asahi, T. Sagawa, and F. Bassinot (2016), Evolution of the North Pacific Subtropical Gyre during the past 190 kyr through the interaction of the Kuroshio Current with the surface and intermediate waters, *Paleoceanography*, *31*, 1498–1513, doi:10.1002/2015PA002914.

Received 14 DEC 2015
Accepted 18 OCT 2016
Accepted article online 20 OCT 2016
Published online 15 NOV 2016

Evolution of the North Pacific Subtropical Gyre during the past 190 kyr through the interaction of the Kuroshio Current with the surface and intermediate waters

Yurika Ujiié[1], Hirofumi Asahi[2], Takuya Sagawa[3], and Franck Bassinot[4]

[1]Center for Advanced Marine Core Research, Kochi University, Nankoku, Japan, [2]Korea Polar Research Institute, Incheon, South Korea, [3]Institute of Science and Engineering, Kanazawa University, Kanazawa, Japan, [4]Laboratoire des Sciences du Climat et de l'Environnement, CNRS-CEA-IPSL Domaine du CNRS, Gif-sur-Yvette, France

Abstract The North Pacific Subtropical Gyre (NPSG) has two important functions, i.e., one in ocean heat transfer and another as a driving force for circulation of the surface and intermediate waters on the basin scale. In the present study, we describe records of the vertical thermal structures and distributions of water masses in the upper ocean of the subtropical northwest (NW) Pacific for the past 190 kyr, using two sediment cores collected from the Kuroshio Current area in the East China Sea and the NPSG area. During the two glacial periods, the Kuroshio Current was weakened owing to changes in ocean-atmosphere circulation and eustasy. The differences in the Mg/Ca-derived temperatures between surface and thermocline waters show the changes of depth and temperature (warming) of thermocline during glacial periods. Conversely, the planktonic foraminiferal assemblages demonstrate that the indicator of the intermediate water from the central area of the NPSG increased synchronously with thermocline warming during marine isotope stage (MIS) 6. These results suggest that warm intermediate water strongly affected the changes in the water-column structure of the subtropical NW Pacific during MIS 6. However, during MIS 2, cold water had precedence over intermediate water probably owing to the southward shift of the subtropical front associated with the reduced transport of the Kuroshio Current. Thus, the NPSG has evolved differently during the two glacial periods (MIS 2 and MIS 6) through interactions between the Kuroshio Current, surface water, and intermediate water.

1. Introduction

The North Pacific Subtropical Gyre (NPSG) plays important roles in heat transportation through the oceans and to the atmosphere and in advection of intermediate and subtropical-mode waters. The Kuroshio Current, which flows along the western margin of the NPSG, carries ocean heat stored in the Western Pacific Warm Pool (WPWP) into high-latitude areas and the central part of the North Pacific basin [*Kelly et al*., 2010] (Figure 1a). In the deeper layer, the North Pacific Intermediate Water (NPIW) comes around the NPSG margin via the Kuroshio Extension and California Current and enters the North Pacific basin [*You*, 2003]. The subtropical-mode water formation takes place in the south area of the Kuroshio Extension and is dependent upon the intensity of the northeast wind and the transport of the Kuroshio Current; subsequently, this cold dense water sinks down to 100–400 m water depth in the subtropical area of the NW Pacific Ocean [*Masuzawa*, 1969; *Hanawa and Talley*, 2001; *Yasuda and Kitamura*, 2003]. Thus, the Kuroshio Current affects the ocean structure from the surface to intermediate waters in the NW Pacific.

In the modern ocean, because the Kuroshio Current has a long path from the equator to middle-latitude areas, its route and transport are affected by multiple regional and remote forcings (e.g., the Asian Monsoon and El Niño–Southern Oscillation (ENSO)) in each latitudinal zone [*Qiu and Lukas*, 1996; *Kawabe*, 2001; *Hwang and Kao*, 2002]. During glacial periods, the intensities of the East Asian summer and winter monsoons were markedly changed [e.g., *Rousseau et al*., 2009; *Cheng et al*., 2009]. The WPWP, which is an ocean heat source in the Pacific, varied in relation to the ENSO state during the last glacial period [e.g., *Stott et al*., 2002; *Koutavas et al*., 2002]. Moreover, reconstruction of the past thermocline depth showed that the water-column structure in the equatorial Pacific was altered in association with the intensity of the Walker circulation [*de Garidel-Thoron et al*., 2007; *Bolliet et al*., 2011; *Sagawa et al*., 2012]. These glacial changes in both the atmosphere and the equatorial Pacific could have affected the condition of the Kuroshio Current. On the other hand, long-term paleotemperature records in the WPWP showed that the mean temperature of

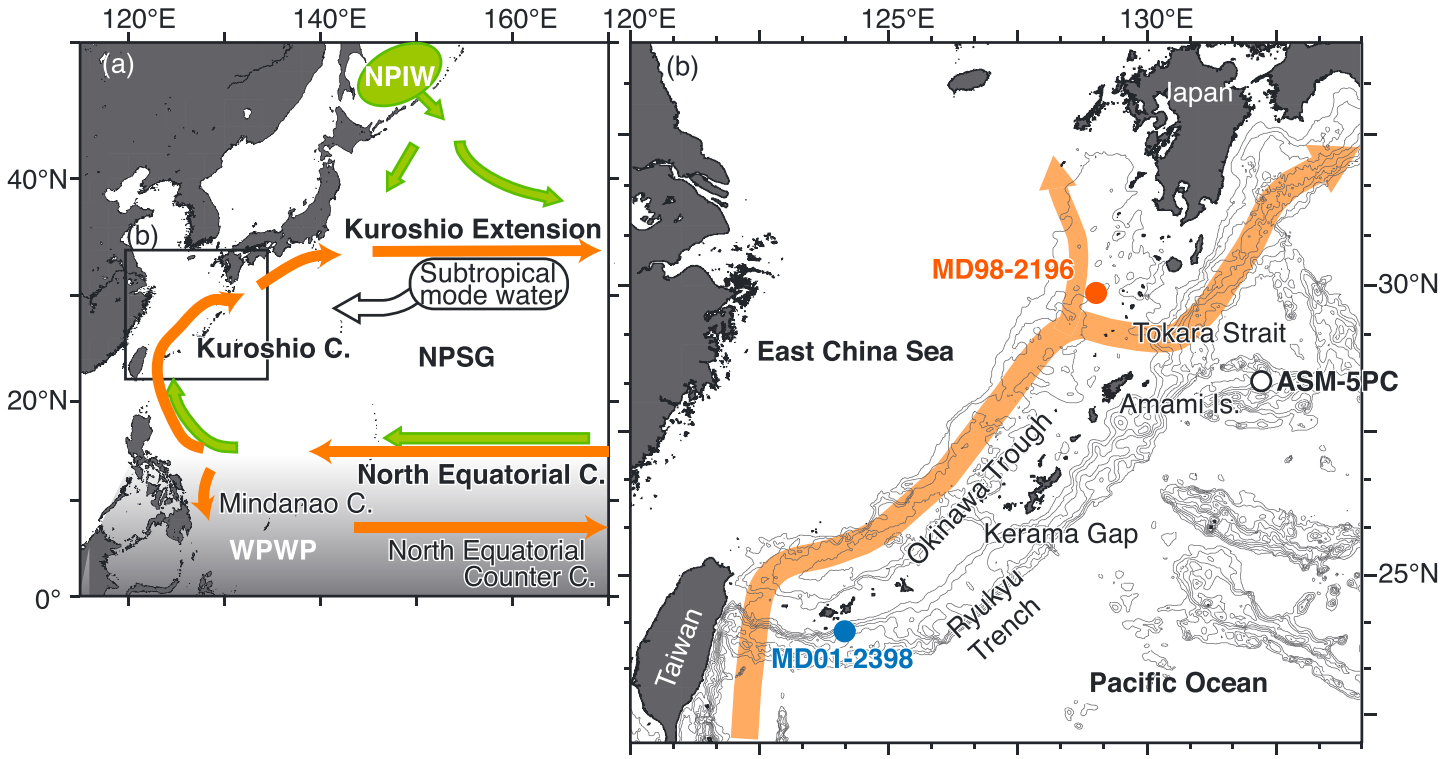

Figure 1. (a) Map of ocean circulation in the NW Pacific Ocean. The surface currents in the NPSG and equatorial areas are indicated by orange arrows. The NPIW is formed in the Okhotsk Sea (green circle) and advects into the NW Pacific following the directions shown by the green arrows. The subtropical-mode water, formed in the south area of the Kuroshio Extension (white circle), advects westward (white arrow). (b) Ocean floor topography of the Ryukyu Islands region. The sites of two studied cores (MD98-2196 and MD01-2398) and the reference core (ASM-5PC) are shown as red, blue, and white circles, respectively. The orange arrow indicates the main path of the Kuroshio Current.

subsurface water tended to decrease through the last 800 kyr, probably due to advection of subtropical and intermediate waters [*Regoli et al.*, 2015]. Direct evidence of the NPSG evolution through multiple glacial-interglacial (G/IG) cycles is required to assess the contribution of the subtropical area to global climate change.

For paleoceanographic reconstruction in the NPSG area, it is important to consider all the geographic characteristics of the marginal seas. In addition to atmospheric and oceanic forcings, eustatic changes also affect the path of the Kuroshio Current because this current flows along a marginal sea surrounded by a complex frame of continents and islands [*Kelly et al.*, 2010]. Today, the Kuroshio Current flows into the East China Sea (ECS) through a gap between islands and out through the Tokara Strait around the northern Okinawa Trough (Figure 1b). Previous studies showed that the sill of this gap became shallow because of low sea level and consequently impeded the Kuroshio inflow to the ECS during the last glacial period [e.g., *Ujiié and Ujiié*, 1999; *Ujiié et al.*, 2003]. Then, the main stream of the Kuroshio Current possibly moved from the ECS to the Pacific side [*Ujiié and Ujiié*, 1999], and other water masses replaced the Kuroshio water in the ECS [*Ujiié et al.*, 2003]. In the 3-D ocean model, shoaling of the sill depth reduced the Kuroshio inflow to the ECS and the main stream flowed out at the Kerama Gap, the central Okinawa Trough [*Kao et al.*, 2006]. The eustatic change around the ECS was clearly suggested by the observation of a stepwise warming following sea level rise during the last deglaciation [*Kiefer and Kienast*, 2005]. The glacial path of the Kuroshio Current around the ECS has been repeatedly examined using evidence from sea surface temperature (SST) records [e.g., *Lee et al.*, 2013]. On the basis of small differences of SST between the ECS and Pacific side, *Lee et al.* [2013] suggested that the eustatic change had little effect on the Kuroshio path during the last glacial period. Use of only the SST records, however, is insufficient to decipher past changes in the path and transport of the Kuroshio Current, because the main body of this current is at ~150 m water depth. In order to properly understand the evolution of the Kuroshio Current, investigation of past changes of the

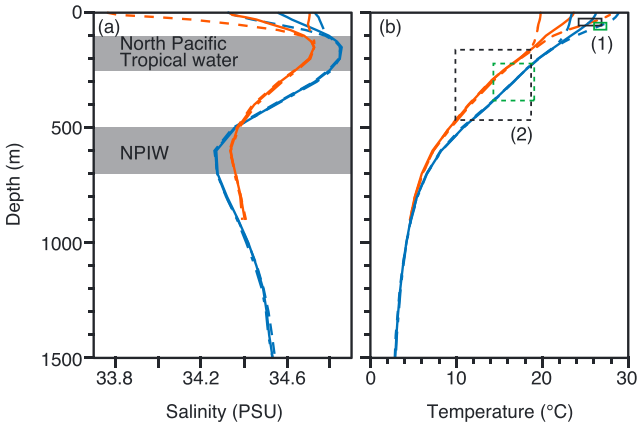

Figure 2. Vertical profiles of (a) salinity and (b) temperature in annual mean (solid line), winter (dashed line), and summer (dotted line) seasons at two core sites: MD98-2196 (red color) and MD01-2398 (blue color). The data were obtained from the World Ocean Atlas 2005 [*Locarnini et al*., 2006]. The salinity profile of core MD01-2398 indicates the zones of salinity minimum and maximum, which are associated with the NPIW and North Pacific Tropical water, respectively [*Nitani*, 1972; *Masuzawa*, 1972]. Boxes in black (MD98-2196) and green (MD01-2398) show the average Mg/Ca temperatures during the Holocene: (1) *G. ruber* and (2) *G. inflata*.

upper ocean structure between the surface and bottom of the thermocline (i.e., the uppermost part of the intermediate water) is necessary.

The present study documents the complete record of the upper ocean structure over the last 190 kyr covering two G/IG cycles in the subtropical NW Pacific area for the first time. We used two long cores, one from the ECS and another from the Pacific Ocean, to monitor the environmental changes of the Kuroshio Current and NPSG area. These two cores could be used to reveal the geographic changes peculiar to the marginal sea resulting from glacial eustasy. Vertical gradients of water temperature were estimated from the Mg/Ca-derived temperatures of two planktonic foraminiferal species, one that dwells in surface water and another that dwells in thermocline water. The effects of the Kuroshio Current and water masses were estimated by analysis of planktonic foraminiferal assemblages.

2. Oceanographic Setting

The NPSG rotates clockwise from the low to middle latitudes of the North Pacific Ocean. The Kuroshio Current diverges from the North Equatorial Current around 15°N (east of the Philippine Islands) and flows along the west margin of the NPSG [*Nitani*, 1972] (Figure 1a). The main part (upper ~500 m water depth) of the Kuroshio Current enters the ECS through a gap (maximum depth: ~800 m) between the south Ryukyu Islands and Taiwan and flows along the outer edge of the continental shelf toward the Tokara Strait (>1000 m depth) (Figure 1b). After the Tokara Strait, the Kuroshio Current flows northeastward until ~37°N, where the stream extends eastward as the Kuroshio Extension.

The path and transport of the Kuroshio Current show variations in the ECS, South of Japan, and Kuroshio Extension areas. In the ECS, the Kuroshio Current flows near the shore with weak transport in fall and far from shore with strong transport in summer, although there are small variations [*Liu and Gan*, 2012]. On the other hand, the Kuroshio Current largely meanders South of Japan depending on its transport, in addition to the upstream path around the Tokara Strait [e.g., *Kawabe*, 1995]. The path of the Kuroshio Extension shows a north-south shift depending on the Kuroshio transport; a large transport results in a northward shift of its path, and a small transport leads to a southward shift [*Qiu*, 2002]. Moreover, the large Kuroshio transport from the South of Japan to the extension area intensifies the southern recirculation gyre leading to westward advection of the intermediate water [*Qiu*, 2002; *Qiu and Chen*, 2005]. A strong recirculation of the gyre increases the heat storage in the south area of the Kuroshio Extension [*Vivier et al*., 2002]. When the northeasterly wind removes this large heat from the surface water, the cold dense water sinks down to deeper than 100 m water depth and is advected southwestward as the subtropical-mode water.

The water-column structure in the subtropical NW Pacific is principally defined by the interaction between two water masses: the North Pacific Tropical Water and NPIW, as shown in the vertical salinity profile of the water column at the site of core MD01-2398 (Figure 2a). The North Pacific Tropical Water is characterized by high-salinity water between 100 and 250 m water depth, whereas the NPIW is characterized by low-salinity water between 500 and 700 m water depth [*Nitani*, 1972; *Masuzawa*, 1972]. In the ECS, low-salinity water moves from the Huanghe and Yangtze Rivers to the Okinawa Trough during summer [e.g., *Katoh et al*., 1996]. This riverine freshwater controls the seasonal salinity of the surface water in the ECS, as is apparent

in the vertical salinity profile of the water column at the site of core MD98-2196 (Figure 2a). Meanwhile, the permanent thermocline ranges between 150 and 550 m water depth depending on the mixing intensity of the Kuroshio Current [*Oka and Kawabe*, 1998]. Temperature and salinity profiles show seasonal changes in the uppermost ~100 m water depth and the permanent thermocline between ~150 and ~500 m water depth at the two sampling sites of cores MD98-2196 and MD01-2398 (Figures 2a and 2b).

3. Material and Methods

3.1. Core Lithology and Chronology

The two cores used in this study were obtained from the subtropical NW Pacific region (Figure 1b): core MD98-2196 was collected from the Okinawa Trough in the ECS (29°52.58′N, 128°36.50′E, 951 m water depth); core MD01-2398 was collected from the south Ryukyu Trench in the Pacific Ocean (23°59.51′N, 124°24.76′E, 2140 m water depth). The sediments in these cores are generally composed of homogeneous clay to silty clay with several volcanic ash layers.

The stratigraphy of each core was assessed on the basis of the stable oxygen isotope ratios ($\delta^{18}O$) of the planktonic foraminifer *Globigerinoides sacculifer* [*Ujiié and Ujiié*, 2006]. Cores MD98-2196 and MD01-2398 cover the time intervals from the end of marine isotope stage (MIS) 7 to the Holocene and from MIS 12 to the Holocene, respectively. The chronologies of the two cores were obtained by graphic correlation to the reference curve LR04 [*Lisiecki and Raymo*, 2005] and accelerator mass spectrometer (AMS) ^{14}C ages, which were obtained from two and six layers in cores MD98-2196 and MD01-2398, respectively (Table S1 in the supporting information). The AMS ^{14}C ages were measured from planktonic foraminiferal shells of *Neogloboquadrina dutertrei* for core MD98-2196 and *G. sacculifer* for core MD01-2398 and were converted into calendar ages by using the MARINE13 calibration curve in the CALIB 7 radiocarbon calibration program [*Reimer et al.*, 2013] without ΔR correction. The average sedimentation rates were 30.4 cm/kyr during glacial periods and 16.9 cm/kyr during interglacial periods in core MD98-2196. In core MD01-2398, the average sedimentation rate was 8.5–9.5 cm/kyr with no significant differences between glacial and interglacial periods. In the present study, we compare the results for the time interval from the beginning of MIS 6 to the Holocene.

3.2. Calcification Depths of Planktonic Foraminifera

Previous studies estimated the calcification depths of planktonic foraminifera based on comparisons of the oceanographic profiles with the $\delta^{18}O$ or Mg/Ca-derived temperatures of planktonic foraminiferal shells obtained from core tops, cores, plankton nets, and sediment traps. From tropical to temperate areas, the calcification depths of *Globigerinoides ruber* and *G. sacculifer* are associated with the surface water (~50 m water depth) [e.g., *Patrick and Thunell*, 1997; *Cléroux et al.*, 2007]. On the other hand, most globorotaliid species dwell in waters deeper than the surface [*Bé*, 1977; *Hemleben et al.*, 1989]. The calcification depth of *Globorotalia inflata* is associated with the thermocline in the tropical Pacific [*Patrick and Thunell*, 1997], the Pacific sector of the Southern Ocean [*Mortyn and Charles*, 2003; *Tapia et al.*, 2015], and the Atlantic Ocean [e.g., *Wilke et al.*, 2006; *Cléroux et al.*, 2007; *Groeneveld and Chiessi*, 2011; *Friedrich et al.*, 2012]. These depths range widely between 50 and 400 m water depth depending on the water-column structure [*Wilke et al.*, 2006]. In the Okinawa Trough, the calcification depth of *G. inflata* is estimated on the basis of $\delta^{18}O$ measurements by using the two surface sediment and one core top samples [*Kubota et al.*, 2012]. In their measurements of each of 63 specimens, the $\delta^{18}O$ of *G. inflata* mostly ranged between +0.3 and −0.4‰. These $\delta^{18}O$ values were associated with the equilibrium $\delta^{18}O_{calcite}$, which ranged between 150 and 450 m [*Kubota et al.*, 2012]. Consequently, the calcification depth of *G. inflata* is associated with the thermocline, and its depth is shifted according to the thermocline depth. In the present study, those three species, *G. sacculifer*, *G. ruber*, and *G. inflate*, were continuously found in the two studied cores. We used these species for the $\delta^{18}O$ and Mg/Ca measurements as indicators of surface and thermocline waters.

3.3. Stable Isotope Analysis

In addition to $\delta^{18}O_{sac}$ curves of *G. sacculifer*, $\delta^{18}O$ of *G. inflata* ($\delta^{18}O_{inf}$) was measured at 2–3 kyr intervals in both cores. We picked 20–30 specimens per sample in the >150 μm size fraction and gently crushed them into large fragments. These fragments were cleaned by sonication in Milli-Q water and methanol and dried at room temperature in a clean drying cabinet overnight. The measurement was conducted using a GV Instruments IsoPrime mass spectrometer with MultiCarb system at Kochi University, Nankoku, Japan. The

analytical error was estimated to be ±0.06‰ for $\delta^{18}O$ (1σ) from repeated measurements of standard material NBS-19.

3.4. Mg/Ca Analyses

Mg/Ca measurements were performed on two species, *G. ruber* and *G. inflata*, at 1–2 kyr intervals in both cores. For each sample, we picked 20–30 specimens in the 250–355 μm size fraction for *G. ruber* and in the >150 μm size fraction for *G. inflata*. To clean the foraminiferal shells, we followed the protocol of *Sagawa and Ikehara* [2008], which included reductive, oxidative, and weak acid-leaching steps in addition to cleaning with ultrasonication in Milli-Q water and methanol. Cleaned samples were dissolved in 75 mM HNO_3. These solutions were diluted to equal ~10 ppm of calcium concentration to reduce matrix effects. The elemental ratios of Mg, Sr, Fe, and Mn to Ca were determined by the intensity calibration method [*de Villiers et al*., 2002] using an inductively coupled plasma atomic emission spectroscopy (PerkinElemer® Optima4300DV CYCRON) at Kochi University. The analytical error was ±1% for Mg/Ca (1σ).

The Mg/Ca values of both *G. ruber* and *G. inflata* were converted to temperatures using the calibration equation (Mg/Ca = 0.38 × exp (0.09 × temperature)), which was proposed for multiple species by *Anand et al*. [2003]. Other equations have been proposed to adjust for different species [*Hastings et al*., 2001; *Anand et al*., 2003] and exclude the effect of carbonate dissolution [*Dekens et al*., 2002]. The studied cores were obtained from seafloor shallower than the present depth of the lysocline (2500–3000 m water depth) in the equatorial Pacific [*Pälike et al*., 2012]. Moreover, *Bordiga et al*. [2013] investigated the changes in calcite dissolution from MIS 11 to the present at the Shatsky Rise, which has a water depth (2387 m) similar to that of core MD01-2398 (2140 m), suggesting no significant effect of calcite dissolution after MIS 6. In the present study, therefore, we did not use the calibration equation of *Dekens et al*. [2002]. Moreover, each equation has oriented biases. In order to examine differences in temperature between the sea surface and the thermocline, the use of the same equation for both species (*G. ruber* and *G. inflata*) could reduce such biases.

3.5. Planktonic Foraminiferal Assemblages

Samples for planktonic foraminiferal assemblages were selected at 1–2 kyr intervals in each core, incorporating the present study with *Ujiié and Ujiié* [2006]. We picked all specimens (~300 specimens) of planktonic foraminifera from >150 μm fragments in each sample, which was from one-quarter aliquots of the sieved residues of 2.5 cm^3 sediments. Forty species of planktonic foraminifera were identified in the present study based on the classification in *Ujiié and Ujiié* [2000]. Some species were united into three separate counting groups as follows: (1) the *Pulleniatina* group was composed of *Pulleniatina obliquiloculata* (Parker and Jones), *Pulleniatina finalis* Banner and Blow, and *Pulleniatina okinawaensis* Natori; (2) the *Globigerina bulloides* group included *Globigerina bulloides* d'Orbigny and *Globigerina foliata* Bolli; and (3) the *G. ruber* group consisted of *G. ruber* sensu stricto, *Globigerinoides cyclostomus* (Galloway and Wissler), and *Globigerinoides pyramidalis* (van der Broeck). The specimens of both *Neogloboquadrina pachyderma* and *Neogloboquadrina incompta* were right-coiled forms in the present study. We classified specimens bearing a remarkable lip structure on the aperture as *N. incompta*.

Fourteen and fifteen species were dominant (>1% of average relative abundance) in down-core samples of cores MD98-2196 and MD01-2398, respectively (Table 1). Eleven species were commonly dominant in both cores. *Ujiié and Ujiié* [2000] conducted Q- and R-mode factor analyses of planktonic foraminiferal assemblages in 55 surface sediment samples around the ECS and defined four groups in association with water masses. However, their study was insufficient to assess the faunas in the central and northern parts of the NPSG and lacked some species that were dominant in the present study. We reclassified the dominant species into five faunal groups based on the available studies, which assessed the geographic distributions of modern or living specimens of planktonic foraminifera in the NW Pacific Ocean, as mentioned below.

1. The "tropical/subtropical surface water" indicator is composed of eight species. Four species (*G. ruber*, *G. sacculifer*, *Globigerinoides tenellus*, and *Globigerinella aequilateralis*) were classified into the tropical/subtropical group [*Ujiié and Ujiié*, 2000]. Two species, *Globigerinoides conglobatus* and *Globigerinita glutinata*, were added to this group because they are typically found in the tropical and subtropical Pacific waters [*Bradshaw*, 1959]. *Globoturborotalia rubescens* and *Orbulina universa*, which were distributed from tropical to temperate areas [*Bradshaw*, 1959; *William et al*., 1980], were added to this group, although the relative abundances of both species were less than 2% in down-core analyses.

Table 1. List of Faunal Groups That Indicate Water Masses[a]

Water Mass	Species Name	Remarks
Tropical/subtropical surface water	***Globigerinoides ruber* s.l.**	
	***Globigerinoides sacculifer* (Brady)**	
	***Globigerinoides tenellus* Parker**	
	***Globigerinita glutinata* (Egger)**	
	***Globigerinella aequilateralis* (Brady)**	
	Globigerinoides conglobatus (Brady)	Dominant in MD01-2398
	Globoturborotalia rubescens (Hofker)	Dominant in MD01-2398
	Orbulina universa d'Orbigny	Dominant in MD98-2196
Cold surface water	***Neogloboquadrina pachyderma* (Ehrenberg)**	
	Neogloboquadrina incompta (Cifelli)	Dominant in MD01-2398
Kuroshio water	***Pulleniatina* group**	
	Globorotalia menardii (Parker, Jones, and Brady)	[b] < 1%
	Globorotalia tumida (Brady)	[b] < 1%
Central water	***Globorotalia inflata* (d'Orbigny)**	
	Globorotalia truncatulinoides (d'Orbigny)	Dominant in MD01-2398
	***Globigerina falconensis* Blow**	
Coastal/upwelling water	***Globigerina bulloides* d'Orbigny**	
	Globigerina quinqueloba Natland	Dominant in MD98-2196
	Globigerinella calida (Parker)	Dominant in MD98-2196
	***Neogloboquadrina dutertrei* (d'Orbigny)**	

[a]Bold text shows dominant species (>1% average relative abundance) in cores MD98-2196 and MD01-2398.
[b]The average relative abundance is less than 1%.

Four species (*G. ruber*, *G. sacculifer*, *G. conglobatus*, and *G. glutinata*), which are abundant in the studied cores, are surface dwellers [*Bé*, 1977; *Hemleben et al*., 1989].

2. The "cold surface water" indicator consisted of two species: *N. pachyderma* (dextral) and *N. incompta* are predominately found in relatively cold waters around Japan [*Takemoto and Oda*, 1997]. Both species mainly dwell in surface water (25–35 m water depth) northeast of Japan [*Sagawa et al*., 2013].
3. The "Kuroshio water" indicator is represented by the *Pulleniatina* group. *Pulleniatina obliquiloculata* is distributed from topical to subtropical areas and is particularly abundant in the tropical Pacific-Indian Oceans [*Bé*, 1977]. In the NW Pacific, this species showed high abundance along the margin of the NPSG including the Kuroshio Current [*Kucera et al*., 2005]. In the ECS, this species was mainly distributed in the Kuroshio Current area separately from the other warm-water species [*Ujiié and Ujiié*, 2000]. Additionally, two species, *Globorotalia menardii* and *Globorotalia tumida*, were included in this group following the grouping of *Ujiié and Ujiié* [2000]. These species were mainly found from tropical to subtropical areas [*Bé*, 1977], though the average relative abundances of both species were slightly less than 1%.
4. The "central water" indicator is composed of three species, *G. inflata*, *Globorotalia truncatulinoides*, and *Globigerina falconensis* [*Bradshaw*, 1959; *William et al*., 1980]. In particular, *G. inflata* and *G. truncatulinoides* are deeper dwellers from the thermocline to intermediate water [e.g., *Bé*, 1977; *Hemleben et al*., 1989; *Friedrich et al*., 2012; *Tapia et al*., 2015]. This indicator is representative of lower thermocline-intermediate waters of the central part of the NPSG.
5. The "coastal/upwelling water" indicator is composed of four species. *G. bulloides* is distributed in marginal seas [*Pflaumann and Jian*, 1999; *Ujiié and Ujiié*, 2000; *Yamasaki and Oda*, 2003], high-productivity areas [e.g., *Bé*, 1977; *Reynolds and Thunell*, 1985; *Kuroyanagi et al*., 2002], and particularly in equatorial and coastal upwelling areas [*Prell and Curry*, 1981; *Pflaumann and Jian*, 1999]. Two other species, *Globigerinella calida* and *Globigerina quinqueloba*, were included in this group, because these species were found near the coastal area around Japan involving the continental shelf of the ECS [*Takemoto and Oda*, 1997; *Xu and Oda*, 1999; *Ujiié and Ujiié*, 2000]. Although *N. dutertrei* was classified as the indicator of the Kuroshio Current in *Ujiié and Ujiié* [2000], this species was dominantly found in the transitional areas of the Kuroshio Extension, California Current, and Peru Current [*Bradshaw*, 1959]. Moreover, a later study demonstrated that this species more reasonably characterizes marginal seas such as the ECS [*Ujiié et al*., 2003]. Therefore, we reclassified *N. dutertrei* from the Kuroshio water indicator to this group.

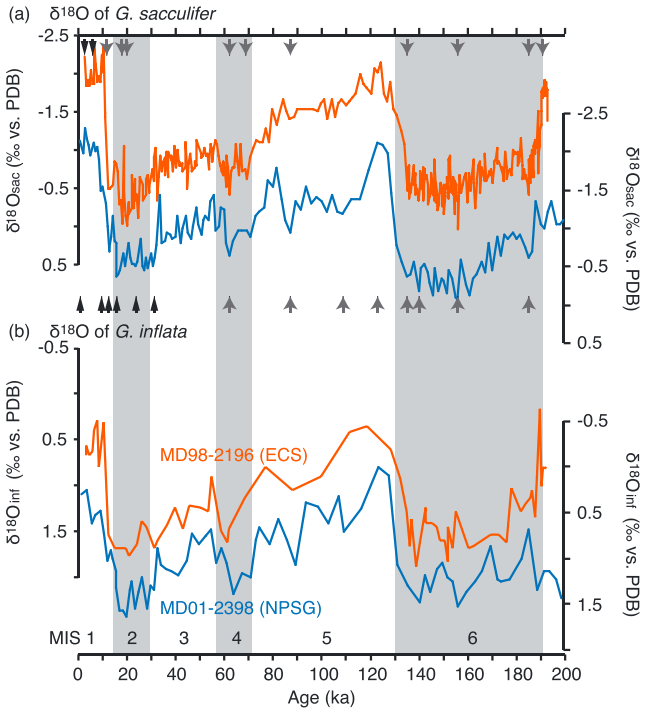

Figure 3. $\delta^{18}O$ curves of two planktonic foraminiferal species, from the (a) surface and (b) thermocline waters, respectively. The curves for each core are shown as red (MD98-2196) and blue (MD01-2398) lines in both panels. Arrows indicate the age-control points based on the AMS ^{14}C ages (black) and $\delta^{18}O$ events (gray), corresponding to Table S1.

4. Results

4.1. Temperature Records

The Mg/Ca-derived temperatures of *G. ruber* and *G. inflata* in the core tops were 25.8 and 10.7°C in core MD98-2196 and 26.5 and 18.9°C in core MD01-2398, respectively. The average temperatures during the Holocene were 25.5°C (*G. ruber*) and 15.2°C (*G. inflata*) in core MD98-2196 and 26.6°C (*G. ruber*) and 16.4°C (*G. inflata*) in core MD01-2398 (Figure 2b). These temperatures are consistent with modern temperatures around 50–75 m and 150–500 m depth in the vertical temperature profiles of the World Ocean Atlas 2005 [*Locarnini et al.*, 2006] (Figure 2b). The $\delta^{18}O_{inf}$ values during the Holocene ranged between +0.28 and +0.79‰ (Figure 3b). In a comparison of these values with the equilibrium $\delta^{18}O_{calcite}$ in *Kubota et al.* [2012], the calcification depth of the studied specimens was estimated between 250 and 420 m water depth. Thus, the Mg/Ca-derived temperatures of *G. ruber* and *G. inflata* represent the temperatures near the sea surface and in the thermocline, congruent with their dwelling depths. When the three other calibration equations of *Hastings et al.* [2001], *Dekens et al.* [2002], and *Anand et al.* [2003] (*G. ruber* specific) were used to convert the Mg/Ca values to temperatures, the Mg/Ca-derived temperatures of *G. ruber* differed by approximately ±2.0°C from those of the equation for multiple species of *Anand et al.* [2003] (Figure S1a). The temperatures calculated by the four different equations were almost parallel to the Mg/Ca values (Figure S1b). In the case of *G. inflata*, the temperatures obtained using the equation for multiple species were lower than those of the species-specific equation (Figure S1c), and the differences widened with increasing temperature (Figure S1d). The temperatures calculated from the two different equations showed differences of more than 4°C for Mg/Ca values greater than 2.5 mmol/mol (Figure S1d).

The Mg/Ca-derived SSTs of both cores, MD98-2196 (ECS) and MD01-2398 (NPSG), changed following the general G/IG pattern of $\delta^{18}O_{sac}$ curves (Figures 3a and 4a); however, the timing of SST changes was not coincident with the onsets of glacial and interglacial periods. During MIS 6, the SST started rising from ~150 ka and increased more after ~140 ka in the ECS. In the NPSG, the SST increased sharply from 140 ka after a slightly warm interval between 160 and 140 ka. In contrast to the early warming of late MIS 6, SSTs rapidly decreased after MIS 5.5 (~120 ka) in both places. In particular, SST remained relatively constant from middle MIS 5 to MIS 2 in the NPSG. On the other hand, the SST record showed a slight increase from MIS 4 to MIS 3 and a decrease toward MIS 2 in the ECS. After MIS 2, SSTs continuously increased after ~17 ka into the Holocene in both places. The average SST was ~1°C colder during MIS 5 than during the Holocene only in the NPSG (Table 2). These increases in the average SSTs were ~3°C for both G/IG transitions (MIS 6/5 and MIS 2/1) in the ECS, whereas they were only 0.8°C for MIS 6/5 and 2.7°C for MIS 2/1 in the NPSG.

The Mg/Ca-derived temperature of the thermocline water showed unique changes, the patterns of which were not harmonious with those of the $\delta^{18}O_{sac}$ and $\delta^{18}O_{inf}$ curves in both the ECS and NPSG (Figures 3a, 3b, and 4b). In both cores, the thermocline temperatures increased twice from the middle of MIS 6 to MIS 5 and from MIS 4 to MIS 2. Compared with the early warming of SST in late MIS 6, the thermocline

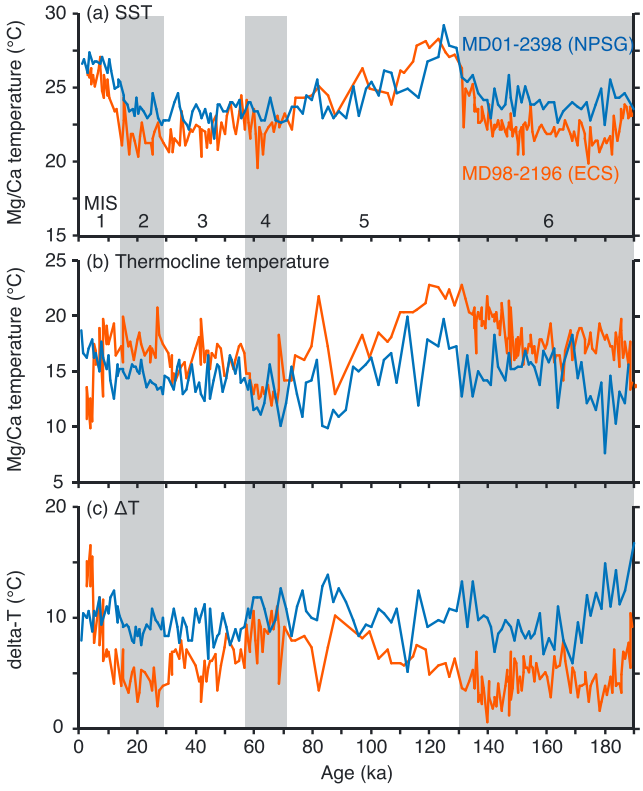

Figure 4. Paleotemperatures estimated from the Mg/Ca values of two planktonic foraminiferal species, representing the (a) surface and (b) thermocline waters. (c) The temperature differences (ΔT) between the surface and thermocline waters are shown. The curves of each core are shown as red (MD98-2196) and blue (MD01-2398) lines in all panels. Gray hatching indicates the glacial periods: MIS 2, 4, and 6.

temperature started increasing much earlier, around ~180 ka, in the NPSG and showed a stepwise increase around ~165 and ~150 ka in the ECS (Figures 4a and 4b). This warm thermocline for MIS 6–5 obviously changed toward MIS 4 with a large temperature drop: 5.2°C in core MD98-2196 and 2.4°C in core MD01-2398 (Table 2).

The ΔT, which is the difference between the SST and the thermocline temperature, was small during MIS 6 and became large toward MIS 4 in both cores (Figure 4c and Table 2). The ΔT turned small from MIS 4 to MIS 2 but was the largest during the Holocene in the ECS. These ΔT changes do not represent conversion bias from the Mg/Ca values to temperatures, because the raw Mg/Ca values of *G. ruber* and *G. inflata* also showed small differences during MIS 6 and MIS 4–2 (Figure S2). Thus, ΔT was greatly affected by warming of thermocline water (Figures 4b and 4c). In particular, the amplitude of ΔT was bigger in the ECS (~6°C) than in the NPSG (~2°C) (Table 2), because the thermocline temperature was markedly altered.

4.2. Planktonic Foraminiferal Assemblages

Changes in the relative abundances of two faunal indicators, representatives of "tropical/subtropical" and "cold" surface waters, were associated with SST changes at each site (Figures 4a, 5a, and 5b). The relative abundance of the cold surface water indicator started decreasing from the middle MIS 6 and showed a lower abundance during MIS 6 than during MIS 2. In contrast, the relative abundance of the tropical/subtropical surface water indicator tended to increase from the middle MIS 6. This faunal indicator persisted at a similar abundance from MIS 5 to MIS 2 and increased from MIS 2 to the Holocene.

Table 2. Average Values of Sea Surface Temperature (SST), Thermocline Temperature (T_{thermo}), and Temperature Differences (ΔT) Between Surface and Thermocline Waters in Cores MD98-2196 and MD01-2398 During Each Period[a]

	MIS 1	MIS 2	LGM	MIS 3	MIS 4	MIS 5	MIS 6	Middle of MIS 6
Period (ka)	0–14	14–29	18–25	29–57	57–71	71–130	130–191	145–180
				Core MD98-1296				
SST (°C)	25.3 [18]	21.7 [18]	21.3 [6]	22.0 [32]	22.2 [18]	25.6 [22]	22.5 [105]	21.9 [51]
T_{thermo} (°C)	15.5 [19]	17.3 [19]	17.1 [7]	16.0 [30]	13.7 [18]	18.9 [22]	17.8 [103]	17.3 [49]
ΔT (°C)	9.9 [17]	4.2 [17]	3.9 [6]	6.0 [30]	8.5 [18]	6.7 [22]	4.8 [97]	4.6 [48]
				Core MD01-2398				
SST (°C)	26.2 [16]	23.5 [19]	23.4 [9]	23.3 [26]	23.2 [10]	24.9 [26]	24.1 [39]	24.0 [23]
T_{thermo} (°C)	15.9 [17]	14.5 [19]	14.9 [9]	14.3 [26]	12.4 [10]	14.6 [26]	14.2 [40]	15.0 [23]
ΔT (°C)	10.3 [16]	9.0 [19]	8.5 [9]	8.9 [26]	10.8 [10]	10.3 [26]	9.9 [39]	9.0 [23]

[a]The LGM was from 25 to 18 ka; the middle MIS 6 was from 180 to 145 ka. The number in square brackets are the numbers of samples. LGM, Last Glacial Maximum.

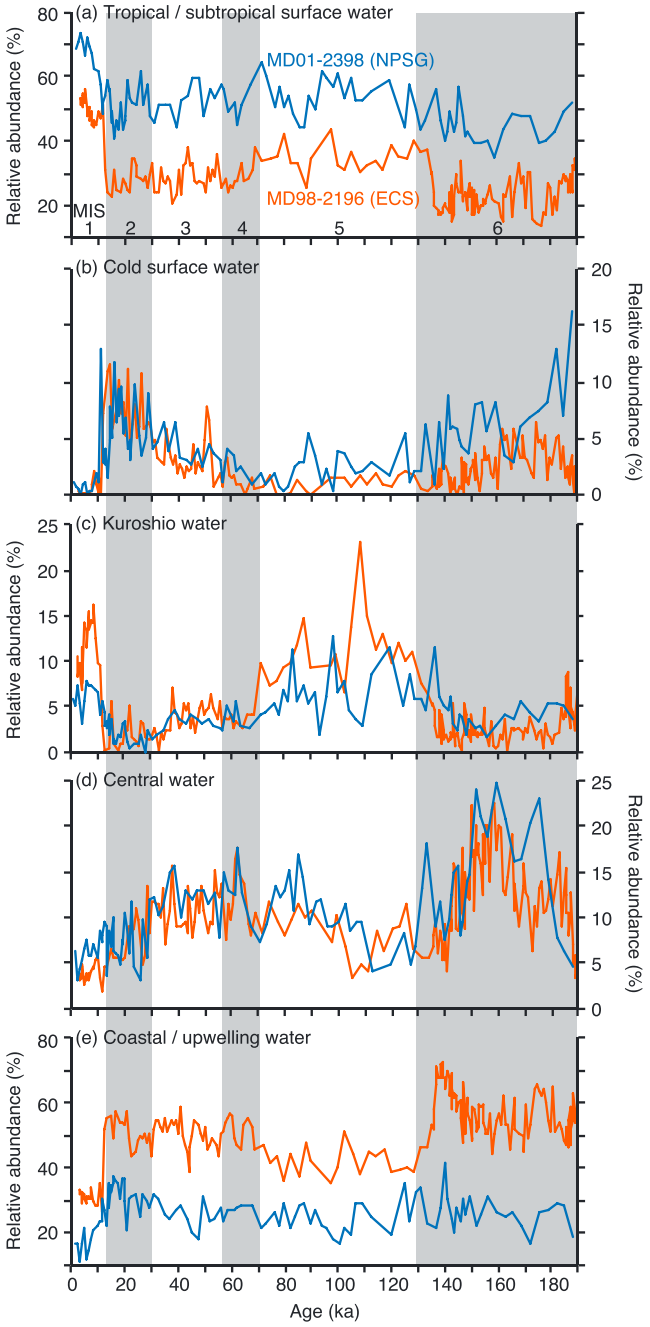

Figure 5. Down-core variations in relative abundance of the faunal indicators based on the planktonic foraminiferal assemblages: (a) tropical/subtropical surface, (b) cold surface water, (c) Kuroshio, (d) central water. and (e) coastal/upwelling water. The curves of each core are shown as red (MD98-2196) and blue (MD01-2398) lines in all panels. Gray hatching indicates the glacial periods: MIS 2, 4, and 6.

Changes in the faunal indicator for Kuroshio water were clearly coincident with the G/IG cycles of the $\delta^{18}O_{sac}$ curve, particularly in the ECS (Figures 3a and 5c). When the Kuroshio water indicator decreased during MIS 6 and MIS 4–2, two other indicators, cold surface water and central water, increased in both cores (Figures 5b–5d). The central water indicator started increasing after the decrease in the cold surface water indicator around 170–180 ka and increased again from the middle of MIS 5. These two indicators switched in dominance between the two glacial periods; the central water of the NPSG was dominant during MIS 6, whereas the cold surface water was dominant during MIS 2.

In addition to the two faunal indicators of central water and cold surface water, the "coastal water" indicator increased during MIS 6 and MIS 4–2 in the ECS (core MD98-2196) (Figure 5e). In particular, this indicator displayed a high peak in the late MIS 6 just before MIS 6/5.

5. Discussion

5.1. Changes in Water Temperature

In our study area (ECS and NPSG), the SSTs were relatively warmer during MIS 6 than during MIS 2 (Figure 4a and Table 2). A similar warm state during MIS 6 has been observed in the WPWP [*Bolliet et al.*, 2011], east equatorial Pacific [*Lea et al.*, 2000, 2002], off New Zealand [*Pahnke et al.*, 2003], and southeast of Australia [*Tachikawa et al.*, 2009]. The warm peak around 160–150 ka has been widely detected from the equator to midlatitude areas in the Pacific Ocean but not in the Vostok ice core record [*Petit et al.*, 1999]. Based on this geographically limited distribution of the pre-deglacial warm peak, *Pahnke et al.* [2003] suggested that this warm anomaly was driven by Northern Hemisphere insolation. Moreover, warm and humid conditions were detected from the $\delta^{18}O$ record of stalagmites and faunal changes in terrestrial mollusks from Chinese loess deposits around 180 ka [*Rousseau et al.*, 2009; *Cheng et al.*, 2009]. These continental records indicate that strong summer insolation enhanced the East Asian summer monsoon, with warming in the tropical and subtropical oceans during MIS 6.

In terms of regional SST difference, SST was ~2°C colder in the ECS (core MD98-2196) than in the NPSG (core MD01-2398) during both glacial periods, MIS 6 and MIS 2 (Figure 4a). Although there are no available data for MIS 6 around the ECS, the Mg/Ca-derived SSTs of MIS 2 were estimated for the Okinawa Trough and the side of the Ryukyu Trench [e.g., *Sagawa et al*., 2011; *Lee et al*., 2013]. The SST of MIS 2 in core MD98-2196 was ~2°C colder than that of core ASM-5PC, which was obtained from the Pacific side in the same latitudinal zone [*Sagawa et al*., 2011] (Figures 1b). During MIS 2, the average SSTs of the northern and central Okinawa Trough in the ECS ranged between 22 and 23°C similar to the values of core MD98-2196, whereas the SST of the central Ryukyu Trench in the NPSG was between 23 and 24°C, similar to core MD01-2398 [*Lee et al*., 2013]. Our Mg/Ca-derived SST data together with the previous studies show small regional differences between the Okinawa Trough and the side of the Ryukyu Trench. In contrast to the SST changes, the thermocline temperature increased more during MIS 6–5 and MIS 4–2 in core MD98-2196 (the ECS) than in core MD01-2398 (the NPSG), resulting in a small ΔT (Figures 5b and 5c and Table 2). Considering the dependence of the calcification depth of *G. inflata* on water-column structure [*Wilke et al*., 2006], these ΔT changes suggest vertical migration (deepening or shoaling) of the thermocline depth.

A strong signal of the East Asian winter monsoon was reported during MIS 2 in the ECS [*Ijiri et al*., 2005], the South China Sea [*Steinke et al*., 2010], and the Sulu Sea [*de Garidel-Thoron et al*., 2001]. The intensified monsoonal wind possibly promoted mixing of the surface water in the ECS; subsequently, the thermocline could have become deeper and its temperature could have become closer to the SST. However, east of Amami Island (core ASM-5PC), *Sagawa et al*. [2011] suggested shoaling of the thermocline during MIS 2, based on changes in the Mg/Ca-derived temperature records from three planktonic foraminifera, which dwell separately in the surface, upper thermocline, and lower thermocline waters. Because the lower thermocline water was cold in spite of the warm temperature in the upper thermocline during MIS 2, the cold water derived from the subtropical-mode water flowed into the intermediate layer and could have pushed surface-mixed water upward, hence shoaling the thermocline depth [*Sagawa et al*., 2011]. Thus, the thermocline temperature rather than the SST largely changed during glacial periods in particular in the ECS, suggesting a change in thermocline depth. Although the thermal structure of the water column indicates the opposite possibility (deepening or shoaling) for the glacial thermocline depth, it is necessary to discuss glacial states of the water-column structure considering the geographic distribution of water masses.

5.2. Changes of Water Masses

The relative abundances of the tropical/subtropical surface water indicator displayed their highest values during the Holocene in both the ECS and NPSG (Figure 5a). This indicator increased during MIS 5 but was not as high as during the Holocene. The changes of the tropical/subtropical surface water indicator are congruent with the fluctuation of the SSTs, which rapidly decreased after MIS 5.5 (Figure 4a). On the other hand, the Kuroshio water indicator changed in phase with the G/IG cycles of $\delta^{18}O_{sac}$ rather than the SST (Figures 3a, 4a, and 5c). In particular, the amplitude of this indicator's fluctuation was large at the glacial-interglacial terminations in the ECS. As eustatic changes are generally associated with the G/IG cycles of the $\delta^{18}O$ curve, sea level change could be related to changes in the Kuroshio water indicator. Previous studies suggested that low glacial sea level restricted the inflow of the Kuroshio Current completely [*Ujiié and Ujiié*, 1999] or partly [*Kao et al*., 2006]. Moreover, multiple down-core analyses of the planktonic foraminiferal fauna demonstrated the decrease of the Kuroshio water indicator during MIS 2 in the whole Okinawa Trough [*Ujiié et al*., 2003]. This faunal-based estimation for the glacial Kuroshio Current was questioned by other previous studies [e.g., *Lee et al*., 2013], based mainly on geochemical proxies for SST estimation. However, use of only SST estimation is insufficient to reconstruct paleothermal structure of the water column. In the modern ocean, the strong impact of the Kuroshio Current promotes mixing of the upper water with the deep thermocline [*Oka and Kawabe*, 1998]. Given that the effect of the Kuroshio Current was weakened during glacial periods in the ECS, the glacial Kuroshio Current could have reduced the intensity of mixing in the upper ocean, resulting in a shallow thermocline. The change in thermocline depth is accordingly supported by warming of the thermocline temperature and decreasing of ΔT (Figures 4b and 4c). Data on both temperature and planktonic foraminiferal assemblages strongly suggest that the effect of the Kuroshio Current was weak during glacial periods in the ECS.

When the two indicators, tropical/subtropical surface water and Kuroshio water, decreased during glacial periods, the other three indicators increased. The cold surface water indicator increased during MIS 6 and

MIS 4–2 in accordance with the low SSTs (Figures 4a and 5b). This finding indicates that the study area cooled with the development of the cold surface water during glacial periods. However, the relative abundance of the cold surface water indicator was low during MIS 6 rather than during MIS 2 in the ECS (Figure 5b). This glacial difference could be reflected in the relatively warm SSTs of MIS 6 (Figure 4a and Table 2). In contrast to the cold surface water indicator, the central water indicator showed higher abundance during MIS 6 than MIS 2 (Figure 5d). Indeed, the central water indicator synchronously changed with warming/cooling of the thermocline temperature in the ECS and NPSG (Figures 4b and 5d). This indicated that the intermediate water derived from the central area of the NPSG affected warming of the thermocline temperature during MIS 6 and from middle MIS 5 to MIS 3. Thus, the faunal indicators for water masses suggest shoaling of the thermocline due to advection of intermediate water during MIS 6.

In the ECS, the coastal water indicator increased during glacial periods (Figure 4e). Multiple down-core analyses of the planktonic foraminiferal fauna demonstrated the development of coastal water over the ECS during MIS 2 [*Ujiié et al*., 2003; *Ijiri et al*., 2005]. At the present day, the coastal water is bounded along the edge of the continental shelf of the ECS by the strong flow of the Kuroshio Current [*Oka and Kawabe*, 1998]. When the Kuroshio Current weakened during MIS 2, the coastal water extended over the ECS [*Ujiié et al*., 2003]. Our faunal analyses suggest that the coastal water was distributed over the ECS during MIS 2 and MIS 6. However, the very high peak of *G. bulloides* in the late MIS 6 could indicate another possibility [*Ujiié and Ujiié*, 2006]. This peak appeared just after the increase of the central water indicator, which is composed of the thermocline-intermediate water dwellers. A similar faunal change was reported in the east equatorial Pacific Ocean, although in different periods (MIS 3–2). The relative abundance of *G. bulloides* increased after a high peak of *G. inflata*, because upwelling of nutrient-rich water was induced by advection of the intermediate water [*Martínez et al*., 2003]. Similarly, we propose that nutrient-rich water flowed into the ECS in association with advection of the intermediate water from the central area of the NPSG. Our analytical results of multiple proxies demonstrate that the water-column structure changed mainly corresponding with the effects of the Kuroshio Current and the intermediate water. In the following sections, we discuss the development of water masses and their relationships through the paleoceanographic evolution of the subtropical NW Pacific from MIS 6 to the present day.

5.3. Spatial Changes in the Subtropical Pacific Ocean

5.3.1. MIS 6 to MIS 5

In our study area, the effect of the Kuroshio Current was weak during both glacial periods, MIS 6 and MIS 2–4 (Figure 5c). The greatest difference between these glacial periods was the early warming of the thermocline temperature before the G/IG transition due to the development of the intermediate water from the central water area (Figures 4b and 5d). Moreover, this intermediate water resulted in shoaling of the thermocline (Figures 4b and 4c). Similarly, shoaling of the thermocline in association with the development of the intermediate water was reported during MIS 6 in the Kuroshio Extension area [*Bordiga et al*., 2013]. Although it is not known which intermediate water(s) was developed in the subtropical NW Pacific during MIS 6, at the present day, the NPIW has a strong influence [*Bostock et al*., 2010] and partly advects into the ECS along the margin of the NPSG [*Kaneko et al*., 2001]. The NPIW could have been thick but oligotrophic during the last glacial period [*Matsumoto et al*., 2002]. If the Pacific Meridional Overturning Circulation was enhanced during MIS 6 in the same way as the model simulation for MIS 2 [*Chikamoto et al*., 2012], this circulation system could have supported the development of the intermediate water in the subtropical NW Pacific. However, the lateral advection of the oligotrophic NPIW contradicts the large supply of nutrient-rich water to the ECS as indicated by the marked increase of *G. bulloides* in the late MIS 6 (Figure 5e). The glacial NPIW was insufficient to lead the ocean environmental changes that we observed during MIS 6 around the subtropical NW Pacific.

During middle MIS 6, paleoclimatological records indicated a strengthened East Asian summer monsoon in association with strong summer insolation [*Rousseau et al*., 2009; *Cheng et al*., 2009]. Strong summer insolation works to melt glaciers during summer and to intensify seasonality controls for the development of sea ice during winter [*Denton et al*., 2005]. The cap of sea ice disrupts heat transfer from the ocean to the atmosphere, leading to colder winters and weakening of the Atlantic Meridional Overturning Circulation [*Toggweiler and Lea*, 2010]. That previous study also suggested that southward shift of the Intertropical Convergence Zone moves the middle-latitude westerlies to high latitude in the Southern Hemisphere through teleconnection, and the westerly winds promote upwelling around Antarctica. This wind-driven

upwelling affects development of the Antarctic Intermediate Water (AAIW). Indeed, in the east equatorial Pacific, the large difference in $\delta^{18}O$ values between surface and thermocline planktonic foraminiferal species indicated the effect of the equatorial undercurrent due to advection of the AAIW during middle MIS 6 (~185 ka) [*Spero et al*., 2003]. This advection also provided nutrient-rich water in the East Pacific as shown by the high accumulation rate of biogenic opal during MIS 6/5 [*Hayes et al*., 2011]. Moreover, the AAIW could have played a role in heat transfer from the Southern Ocean to the tropical Pacific, leading to early warming of SST during middle MIS 6 [*Tachikawa et al*., 2009]. The effect of summer insolation may have induced both early warming of SST and development of the AAIW with supply of nutrient-rich water in the subtropical and tropical Pacific Ocean.

Apart from the effect of the AAIW, the atmospheric forcing related to the summer insolation could have provided nutrient-rich water to the ECS at the end of MIS 6 (~ 135–145 ka). After the strong phase of the East Asian summer monsoon, a high impact of the East Asian winter monsoon was detected at the end of MIS 6 in the terrestrial record [*Rousseau et al*., 2009]. This impact of the East Asian winter monsoon was reflected in the record of primary productivity in the Sulu Sea, in which the primary productivity increased around 135–145 ka [*de Garidel-Thoron et al*., 2001]. Further research on long-term paleoceanographic records would provide understanding of the contributions of the intermediate waters and atmospheric factors to the broad supply of the nutrient-rich water into the subtropical and tropical NW Pacific.

5.3.2. After MIS 5 to MIS 2

Warm states in both the surface and thermocline waters altered to cold states after MIS 5.5 into MIS 4 (Figures 4a and 4b). The small increase of the central water faunal indicator from the middle MIS 5 to MIS 2 (Figure 5d) suggests that the effect of the intermediate water became weaker compared to MIS 6–5. In contrast, the high abundance of the cold surface water indicator during MIS 2 indicates a stronger effect of the cold water relative to MIS 6. Nevertheless, the ΔT and the relative abundance of the Kuroshio water indicate similar states during MIS 2 and MIS 6 (Figures 4c and 5c). These results imply that the intermediate waters and surface water masses were developed differently during MIS 2 and MIS 6.

The structural change of the upper water column occurred concurrently in the subtropical and equatorial Pacific Ocean during MIS 2. Shoaling of the thermocline during MIS 2 was inferred from the change in ΔT between the surface and subsurface or thermocline waters in the WPWP [*de Garidel-Thoron et al*., 2007; *Sagawa et al*., 2012]. This could have been caused by the small east-west tilt of the thermocline in the equator, similar to El Niño events. Oceanographic studies have demonstrated that the bifurcation point of the Kuroshio Current from the North Equatorial Current is geographically shifted during El Niño events, leading to a decrease in the Kuroshio transport [*Qiu and Lukas*, 1996; *Akitomo et al*., 1996; *Kawabe*, 2001]. During MIS 2, the El Niño-like conditions may have been one of the factors to weaken the Kuroshio Current.

Of three cores (MD98-2196, MD01-2398, and ASM-5PC) obtained from the ECS and the western margin of the Pacific (Figure 1b), the temperature in the lower part of thermocline was definitely cold only in core ASM-5PC during MIS 2. A previous study inferred that the cold subtropical-mode water was advected to the east of Amami Island [*Sagawa et al*., 2011]; however, increases in the thermocline temperature in our studied cores (MD98-2196 and MD01-2398) provide conflicting evidence for development of the subtropical-mode water in the ECS and southern Ryukyu Trench. In the modern ocean, the subtropical-mode water is principally advected along the margin of the NPSG, where the Kuroshio Current flows [*Suga and Hanawa*, 1995; *Yasuda and Hanawa*, 1999]. When the Kuroshio Current weakens, its downstream Kuroshio Extension becomes weak and migrates southward [*Kawabe*, 1995; *Qiu and Chen*, 2005]. These changes of the Kuroshio Extension consequently produce a lower intensity of the southern recirculation gyre, which is a driving force for westward advection of the subtropical-mode water [*Qiu*, 2002]. During MIS 2, the subtropical-mode water reached to east of Amami Island (core ASM-5PC), though the weak Kuroshio Current diminished the advection intensity of the subtropical-mode water broadly toward the subtropical NW Pacific. Moreover, the path of the glacial Kuroshio Current, which did not enter the ECS across the southernmost gap of the Ryukyu Islands [*Ujiié et al*., 2003; *Kao et al*., 2006], blocked the westward advection of the subtropical-mode water into the ECS. Consequently, the thermocline temperatures of core MD98-2196 in the ECS and core MD01-2398 in the southern Ryukyu Trench did not display cooling during the last glacial period (Figure 4b). Instead of the cold subtropical-mode water, relatively warm intermediate water intruded into the ECS through

the central and/or northern gaps (>1000 m depth) as shown by the increase in the central water indicator (Figure 5d). However, the advection intensity of the intermediate water could not be the same as during MIS 6.

The dominance of the surface water mass was different in our study area between MIS 2 and MIS 6, as demonstrated by high abundance of the cold surface water indicator during MIS 2. The weak Kuroshio Current leads to reduced transport of the Kuroshio Extension with the southward shift of its path [*Kawabe*, 1995; *Qiu and Chen*, 2005]. Changes in the path and transport of the Kuroshio Extension could enable the southward shift of the subtropical front. Under a weakened system of the Kuroshio Current and its extension during MIS 2, the cold surface water may have extended southward following the shift of the subtropical front. Both global and regional changes in the ocean-atmosphere interaction and eustasy promoted glacial conditions in the subtropical NW Pacific.

6. Conclusions

The present study shows the long-term paleoceanographic record (~190 ka) of the subtropical NW Pacific Ocean based on a comprehensive analysis of (i) the Mg/Ca-derived temperatures in surface and thermocline waters and (ii) the planktonic foraminiferal indicators for water masses. The effect of the Kuroshio Current is entirely associated with the G/IG cycles of the $\delta^{18}O$ in the ECS. This relationship shows that the inflow of the Kuroshio Current was impeded due to geographic changes of the marginal sea associated with glacial eustasy during glacial periods. In contrast, changes of the SST and thermocline temperature are not consistent with each other, because the thermocline water warmed up during glacial periods in both the ECS and NPSG areas. In particular, the thermocline temperature obviously started to increase at about 180 ka during MIS 6 to MIS 5.5, and the effect of the intermediate water from the central area of the NPSG accordingly became stronger. The relatively warm intermediate water widely advected into the subtropical NW Pacific with the positive anomaly of summer insolation, preceding warm environment in the upper ocean. The increases in both the SST and tropical/subtropical surface water indicator followed this warm state. However, the SST and thermocline temperature began to decrease about middle MIS 5, and the thermocline water slightly warmed during MIS 4–2. The effect of the warm intermediate water was weaker during MIS 2 than during MIS 6. Instead, cold surface water occurred over the study area during MIS 2. Moreover, cold subtropical-mode water was developed from the Kuroshio Extension area to the northern Ryukyu Trench as a result of ocean-atmospheric interactions in El Niño-like conditions. At the same time, these ocean-atmospheric changes caused weakening of the Kuroshio Current together with the glacial eustatic change. As the weak Kuroshio Current could inhibit westward advection of the subtropical-mode water, thermocline temperatures were not cold in the ECS and the southern Ryukyu Trench. Thus, the vertical structures of the upper ocean in the ECS and NPSG were largely modified during MIS 6 and MIS 4–2, in each of which water masses are differently activated. Changes in the surface current, surface waters, and intermediate waters interacting with ocean-atmospheric circulation and regional eustasy were the key features controlling development of the subtropical NW Pacific across G/IG cycles.

Acknowledgments
We thank the captain and crew of the R/V *Marion Dufresne*, *the IPEV team*, and all scientist participants of the IMAGES-IV and IMAGES-VII (WEPAMA) cruises for the collection of the samples. We deeply thank Hodaka Kawahata, who fund and organized both cruises for all of Japanese participants. Ken Ikehara, Makoto Okada, and Minoru Ikehara are acknowledged for sampling and analyses. We greatly appreciate Jere H. Lipps for his prereviewing our MS. H.A. is supported by two programs: the Basic Research Program by the Korea Polar Research Institute (grant PE 15062 to Seung-Il Nam) and the Excellent Foreigner Postdoc Invitation Program (grant PE 15220 to Seung-Il Nam). This study was supported by Grant-in-Aide for Young Scientist 23710012 and Scientific Research (C) 26400501 of JSPS. This is LSCE contribution 5919. We will always remember and acknowledge the contribution of two great late scientists, Luejiang Wang and Hiroshi Ujiié, who supported warmly this study. The data used in this study are available from the authors upon request (yujiie@kochi-u.ac.jp).

References

Akitomo, K., M. Ooi, T. Awaji, and K. Kutsuwada (1996), Interannual variability of the Kuroshio transport in response to the wind stress field over the North Pacific: Its relation to the path variation south of Japan, *J. Geophys. Res.*, *101*, 14,057–14,071, doi:10.1029/96JC01000.

Anand, P., H. Elderfield, and M. H. Conte (2003), Calibration of Mg/Ca thermometry in planktonic foraminifera from a sediment trap time series, *Paleoceanography*, *18*(2), 1050, doi:10.1029/2002PA000846.

Bé, A. W. H. (1977), An ecological, zoo-geographical and taxonomic review of Recent planktonic foraminifera, in *Ocean Micropaleontology*, vol. 1, edited by A. T. S. Ramsay, pp. 1–100, Academic Press, London.

Bolliet, T., A. Holbourn, W. Kuhnt, C. Laj, C. Kissel, L. Beaufort, M. Kienast, N. Andersen, and D. Garbe-Schönberg (2011), Mindanao Dome variability over the last 160 kyr: Episodic glacial cooling of the West Pacific Warm Pool, *Paleoceanography*, *26*, PA1208, doi:10.1029/2010PA001966.

Bordiga, M., L. Beaufort, M. Cobianchi, C. Lupi, N. Mancin, V. Luciani, N. Pelosi, and M. Sprovieri (2013), Calcareous plankton and geochemistry from the ODP site 1209B in the NW Pacific Ocean (Shatsky Rise): New data to interpret calcite dissolution and paleoproductivity changes of the last 450 ka, *Palaeogeogr. Palaeoclimatol. Palaeoecol.*, *371*, 93–108.

Bostock, H. C., B. N. Opdyke, and M. J. M. Williams (2010), Characterizing the intermediate depth waters of the Pacific Ocean using $\delta^{13}C$ and other geochemical tracers, *Deep Sea Res., Part I*, *57*(7), 847–859, doi:10.1016/j.dsr.2010.04.005.

Bradshaw, J. S. (1959), Ecology of living planktonic foraminifera in the north and equatorial Pacific Ocean, *Contrib. Cushman Found. Foraminif. Res.*, *10*, 25–64.

Cheng, H., R. L. Edwards, W. S. Broecker, G. H. Denton, X. Kong, Y. Wang, R. Zhang, and X. Wang (2009), Ice age terminations, *Science*, *326*, 248–252, doi:10.1126/science.1177840.

Chikamoto, M. O., L. Menviel, A. Abe-Ouchi, R. Ohgaito, A. Timmermann, Y. Okazaki, N. Harada, A. Oka, and A. Mouchet (2012), Variability in North Pacific intermediate and deep water ventilation during Heinrich events in two coupled climate models, *Deep Sea Res., Part II*, *61-64*, 114–126, doi:10.1016/j.dsr2.2011.12.002.

Cléroux, C., E. Cortijo, J.-C. Duplessy, and R. Zahn (2007), Deep-dwelling foraminifera as thermocline temperature recorders, *Geochem. Geophys. Geosyst.*, *8*, Q04N11, doi:10.1029/2006GC001474.

de Garidel-Thoron, T., L. Beaufort, B. K. Linsley, and S. Dannenmann (2001), Millennial-scale dynamics of the east Asian winter monsoon during the last 200,000 years, *Paleoceanography*, *16*, 491–502, doi:10.1029/2000PA000557.

de Garidel-Thoron, T., Y. Rosenthal, L. Beaufort, E. Bard, C. Sonzogni, and A. C. Mix (2007), A multiproxy assessment of the western equatorial Pacific hydrography during the last 30 kyr, *Paleoceanography*, *22*, PA3204, doi:10.1029/2006PA001269.

de Villiers, S., M. Graves, and H. Elderfield (2002), An intensity ratio calibration method for the accurate determination of Mg/Ca and Sr/Ca of marine carbonates by ICP-AES, *Geochem. Geophys. Geosyst.*, *3*(1), 1001, doi:10.1029/2001GC000169.

Dekens, P. S., D. W. Lea, D. K. Pak, and H. J. Spero (2002), Core top calibration of Mg/Ca in tropical foraminifera: Refining paleotemperature estimation, *Geochem. Geophys. Geosyst.*, *3*(4), 1022, doi:10.1029/2001GC000200.

Denton, G. H., R. B. Alley, G. C. Comer, and W. S. Broecker (2005), The role of seasonality in abrupt climate change, *Quat. Sci. Rev.*, *24*, 1159–1182, doi:10.1016/j.quascirev.2004.12.002.

Friedrich, O., R. Schiebel, P. A. Wilson, S. Weldeab, C. J. Beer, M. J. Cooper, and J. Fiebig (2012), Influence of test size, water depth, and ecology on Mg/Ca, Sr/Ca, $\delta^{18}O$ and $\delta^{13}C$ in nine modern species of planktic foraminifers, *Earth Planet. Sci. Lett.*, *319–320*, 133–145, doi:10.1016/j.epsl.2011.12.002.

Groeneveld, J., and C. M. Chiessi (2011), Mg/Ca of *Globorotalia inflata* as a recorder of permanent thermocline temperatures in the South Atlantic, *Paleoceanography*, *26*, PA2203, doi:10.1029/2010PA001940.

Hanawa, K., and L. D. Talley (2001), Mode waters, in *Ocean Circulation and Climate*, edited by G. Siedler, J. Church, and J. Gould, pp. 373–386, Academic Press, London.

Hastings, D., M. Kienast, S. Steinke, and A. A. Whitko (2001), A comparison of three independent paleotemperature estimates from a high resolution record of deglacial SST records in the tropical South China Sea Eos Trans. AGU, 82(47), Fall Meet. Suppl., Abstract PP12B-10.

Hayes, C. T., R. F. Anderson, and M. Q. Fleisher (2011), Opal accumulation rates in the equatorial Pacific and mechanisms of deglaciation, *Paleoceanography*, *26*, PA1207, doi:10.1029/2010PA002008.

Hemleben, C., M. Spindler, and O. R. Anderson (1989), *Modern Planktonic Foraminifera*, Springer, New York.

Hwang, C., and R. Kao (2002), TOPEX/POSEIDON-derived space–time variations of the Kuroshio Current: Applications of a gravimetric geoid and wavelet analysis, *Geophys. J. Int.*, *151*, 835–847, doi:10.1046/j.1365-246X.2002.01811.x.

Ijiri, A., L. Wang, T. Oba, H. Kawahata, C.-Y. Huang, and C.-Y. Huang (2005), Paleoenvironmental changes in the northern area of the East China Sea during the past 42,000 years, *Palaeogeogr. Palaeoclimatol. Palaeoecol.*, *219*, 239–261, doi:10.1016/j.palaeo.2004.12.028.

Kaneko, I., Y. Takatsuki, and H. Kamiya (2001), Circulation of intermediate and deep waters in the Philippine Sea, *J. Oceanogr.*, *57*, 397–420, doi:10.1023/A:1021565031846.

Kao, S. J., C.-R. Wu, Y. C. Hsin, and M. Dai (2006), Effects of sea level change on the upstream Kuroshio Current through the Okinawa Trough, *Geophys. Res. Lett.*, *33*, L16604, doi:10.1029/2006GL026822.

Katoh, O., K. Teshima, O. Abe, H. Fujita, K. Miyaji, K. Morinaga, and N. Nakagawa (1996), Process of the Tsushima Current formation revealed by ADCP measurements in summer, *J. Oceanogr.*, *52*, 491–507, doi:10.1007/BF02239051.

Kawabe, M. (1995), Variations of current path, velocity, and volume transport of the Kuroshio in relation with the large meander, *J. Phys. Oceanogr.*, *25*, 3103–3117, doi:10.1175/1520-0485(1995)025<3103:VOCPVA>2.0.CO;2.

Kawabe, M. (2001), Interannual variations of sea level at the Nansei Islands and volume transport of the Kuroshio due to wind changes, *J. Oceanogr.*, *57*, 189–205, doi:10.1023/A:1011195224933.

Kelly, K. A., R. J. Small, R. M. Samelson, B. Qiu, T. M. Joyce, Y.-O. Kwon, and M. F. Cronin (2010), Western boundary currents and frontal air–sea interaction: Gulf stream and Kuroshio extension, *J. Clim.*, *23*, 5644–5667, doi:10.1175/2010JCLI3346.1.

Kiefer, T., and M. Kienast (2005), Patterns of deglacial warming in the Pacific Ocean: A review with emphasis on the time interval of Heinrich event 1, *Quat. Sci. Rev.*, *24*, 283–293, doi:10.1016/j.quascirev.2004.02.021.

Koutavas, A., J. Lynch-Stieglitz, T. M. Marchitto, and J. P. Sachs Jr. (2002), El Niño-like pattern in ice age tropical Pacific sea surface, *Science*, *297*, 226–230, doi:10.1126/science.1072376.

Kubota, Y., Tada, R., Kimoto, K., and T. Irino (2012), Oxygen and carbon isotopes of individual planktic foraminifera in the middle Okinawa Trough, in *GSJ Interim Report* [in Japanese], edited by K. Arai, pp. 156–162, National Institute of Advance Industrial Science and Technology, Tsukuba, Japan.

Kucera, M., et al. (2005), Reconstruction of sea-surface temperatures from assemblages of planktonic foraminifera: Multi-technique approach based on geographically constrained calibration data sets and its application to glacial Atlantic and Pacific Oceans, *Quat. Sci. Rev.*, *24*, 951–998.

Kuroyanagi, A., H. Kawahata, H. Nishi, and M. C. Honda (2002), Seasonal changes in planktonic foraminifera in the northwestern North Pacific Ocean: Sediment trap experiments from subarctic and subtropical gyres, *Deep Sea Res., Part II*, *49*, 5627–5645, doi:10.1016/j.palaeo.2008.02.012.

Lea, D. W., D. K. Pak, and H. J. Spero (2000), Climate impact of late Quaternary equatorial Pacific sea surface temperature variations, *Science*, *289*(5486), 1719–1724, doi:10.1126/science.289.5485.1719.

Lea, D. W., P. A. Martina, D. K. Pak, and H. J. Spero (2002), Reconstructing a 350 ky history of sea level using planktonic Mg/Ca and oxygen isotope records from a Cocos Ridge core, *Quat. Sci. Rev.*, *21*(2002), 283–293, doi:10.1016/S0277-3791(01)00081-6.

Lee, K. E., H. J. Lee, J.-H. Park, Y.-P. Chang, K. Ikehara, T. Itaki, and H. Kwon (2013), Stability of the Kuroshio path with respect to glacial sea level lowering, *Geophys. Res. Lett.*, *40*, 1–5, doi:10.1012/grl.50102.

Lisiecki, L. E., and M. E. Raymo (2005), A Pliocene-Pleistocene stack of 57 globally distributed benthic $\delta^{18}O$ records, *Paleoceanography*, *20*, PA1003, doi:10.1029/2004PA001071.

Liu, Z., and J. Gan (2012), Variability of the Kuroshio in the East China Sea derived from satellite altimetry data, *Deep Sea Res., Part I*, *59*, 25–36, doi:10.1016/j.dsr.2011.10.008.

Locarnini, R. A., A. V. Mishonov, J. I. Antonov, T. P. Boyer, and H. E. Garcia (2006), in *World Ocean Atlas 2005, Volume 1: Temperature*, *NOAA Atlas NESDIS*, vol. 61, edited by S. Levitus, pp. 182 , NOAA, Silver Spring, Md.

Martínez, I., L. Keigwin, T. T. Barrows, Y. Yokoyama, and J. Southon (2003), La Niña-like conditions in the eastern equatorial Pacific and a stronger Choco jet in the northern Andes during the last glaciation, *Paleoceanography*, *18*(2), 1033, doi:10.1029/2002PA000877.

Masuzawa, J. (1969), Subtropical mode water, *Deep Sea Res.*, *16*, 463–472, doi:10.1016/0011-7471(69)90034-5.

Masuzawa, J. (1972), Water characteristics of the North Pacific Central Region, in *Kuroshio—Its Physical Aspects*, edited by H. Stommel and K. Yoshida, pp. 95–127, Univ. Tokyo Press, Tokyo.
Matsumoto, K., T. Oba, J. Lynch-Stieglitz, and H. Yamamoto (2002), Interior hydrography and circulation of the glacial Pacific Ocean, *Quat. Sci. Rev.*, *21*, 1693–1704, doi:10.1016/S0277-3791(01)00142-1.
Mortyn, P. G., and C. D. Charles (2003), Planktonic foraminiferal depth habitat and $\delta^{18}O$ calibrations: Plankton tow results from the Atlantic sector of the Southern Ocean, *Paleoceanography*, *18*(2), 1037, doi:10.1029/2001PA000637.
Nitani, H. (1972), Beginning of the Kuroshio: Kuroshio, in *Its Physical Aspects*, edited by H. Stommel and K. Yoshida, pp. 129–163, Tokyo Univ. Press, Tokyo.
Oka, E., and M. Kawabe (1998), Characteristics of variations of water properties and density structure around the Kuroshio in the East China Sea, *J. Oceanogr.*, *54*, 605–617, doi:10.1007/BF02823281.
Pahnke, K., R. Zahn, H. Elderfield, and M. Schulz (2003), 340,000-year centennial-scale marine record of southern hemisphere climatic oscillation, *Science*, *301*, 948–952, doi:10.1126/science.1084451.
Pälike, H., et al. (2012), A Cenozoic record of the equatorial Pacific carbonate compensation depth, *Nature*, *488*, 609–614, doi:10.1038/nature11360.
Patrick, A., and R. C. Thunell (1997), Tropical Pacific sea surface temperatures and upper water column thermal structure during the Last Glacial Maximum, *Paleoceanography*, *12*(5), 649–657, doi:10.1029/97PA01553.
Petit, J. R., et al. (1999), Climate and atmospheric history of the past 420,000 years from the Vostok ice core, Antarctica, *Nature*, *399*, 429–436, doi:10.1038/20859.
Pflaumann, U., and Z. Jian (1999), Modern distribution patterns of planktonic foraminifera in the South China Sea and western Pacific: A new transfer technique to estimate regional sea surface temperatures, *Mar. Geol.*, *156*, 41–83, doi:10.1016/S0025-3227(98)00173-X.
Prell, W. L., and W. B. Curry (1981), Faunal and isotope indices of monsoonal upwelling: Western Arabian Sea, *Oceanol. Acta*, *4*, 91–98.
Qiu, B. (2002), The Kuroshio extension system: Its large-scale variability and role in the midlatitude ocean atmosphere interaction, *J. Oceanogr.*, *58*, 57–75, doi:10.1023/A:1015824717293.
Qiu, B., and R. Lukas (1996), Seasonal and interannual variability of the North Equatorial Current, the Mindanao Current, and the Kuroshio along the Pacific western boundary, *J. Geophys. Res.*, *101*, 12,315–12,330, doi:10.1029/95JC03204.
Qiu, B., and S. Chen (2005), Variability of the Kuroshio extension jet, recirculation gyre, and mesoscale eddies on decadal time scales, *J. Phys. Oceanogr.*, *35*, 2090–2103, doi:10.1175/JPO2807.1.
Regoli, F., T. de Garidel-Thoron, K. Tachikawa, Z. Jian, L. Ye, A. W. Droxler, G. Lenoir, M. Crucifix, N. Barbarin, and L. Beaufort (2015), Progressive shoaling of the equatorial Pacific thermocline over the last eight glacial periods, *Paleoceanography*, *30*, 439–455, doi:10.1002/2014PA002696.
Reimer, P. J., et al. (2013), IntCal13 and Marine13 radiocarbon age calibration curves 0–50,000 years cal BP, *Radiocarbon*, *55*, 1869–1887, doi:10.2458/azu_js_rc.55.16947.
Reynolds, L., and R. C. Thunell (1985), Seasonal succession of planktonic foraminifera in the subpolar North Pacific, *J. Foraminiferal Res.*, *15*, 282–301, doi:10.2113/gsjfr.15.4.282.
Rousseau, D. D., N. Wu, Y. Pei, and F. Li (2009), Three exceptionally strong East-Asian summer monsoon events during glacial times in the past 470 kyr, *Clim. Past*, *5*, 157–169, doi:10.5194/cp-5-157-2009.
Sagawa, T., and K. Ikehara (2008), Intermediate water ventilation change in the subarctic northwest Pacific during the last deglaciation, *Geophys. Res. Lett.*, *35*, L24702, doi:10.1029/2008GL035133.
Sagawa, T., Y. Yokoyama, M. Ikehara, and M. Kuwae (2011), Vertical thermal structure history in the western subtropical North Pacific since the Last Glacial Maximum, *Geophy. Res. Lett.*, *38*, L00F02, doi:10.1029/2010GL045827.
Sagawa, T., Y. Yokoyama, M. Ikehara, and M. Kuwae (2012), Shoaling of the western equatorial Pacific thermocline during the Last Glacial Maximum inferred from multispecies temperature reconstruction of planktonic foraminifera, *Palaeogeogr. Palaeoclimatol. Palaeoecol.*, *346–347*, 120–129, doi:10.1016/j.palaeo.2012.06.002.
Sagawa, T., A. Kuroyanagi, T. Irino, M. Kuwae, and H. Kawahata (2013), Seasonal variations in planktonic foraminiferal flux and oxygen isotopic composition in the western North Pacific: Implications for paleoceanographic reconstruction, *Mar. Micropaleontol.*, *100*, 11–20, doi:10.1016/j.marmicro.2013.03.013.
Spero, H. J., K. M. Mielke, E. M. Kalve, D. W. Lea, and D. K. Pak (2003), Multispecies approach to reconstructing eastern equatorial Pacific thermocline hydrography during the past 360 kyr, *Paleoceanography*, *18*(1), 1022, doi:10.1029/2002PA000814.
Steinke, S., M. Mohtadi, J. Groeneveld, L.-C. Lin, L. Löwemark, M.-T. Chen, and R. Rendle-Bühring (2010), Reconstructing the southern South China Sea upper water column structure since the Last Glacial Maximum: Implications for the East Asian winter monsoon development, *Paleoceanography*, *25*, PA2219, doi:10.1029/2009PA001850.
Stott, L., C. Poulsen, S. Lund, and R. Thunell (2002), Super ENSO and global climate oscillations at millennial time scales, *Science*, *297*, 222–226, doi:10.1126/science.1071627.
Suga, T., and K. Hanawa (1995), The subtropical mode water circulation in the North Pacific, *J. Phys. Oceanogr.*, *25*, 958–970, doi:10.1175/1520-0485(1995)025<0958:TSMWCI>2.0.CO;2.
Tachikawa, K., L. Vidal, C. Sonzogni, and E. Bard (2009), Glacial/interglacial sea surface temperature changes in the Southwest Pacific ocean over the past 360 ka, *Quat. Sci. Rev.*, *28*, 1160–1170, doi:10.1016/j.quascirev.2008.12.013.
Takemoto, A., and M. Oda (1997), New planktic foraminiferal transfer functions for the Kuroshio-Oyashio Current region, *Jpn. Paleontol. Res.*, *1*, 291–310.
Tapia, R., D. Nürnberg, T. Ronge, and R. Tiedemann (2015), Disparities in glacial advection of Southern Ocean Intermediate Water to the South Pacific Gyre, *Earth Planet. Sci. Lett.*, *410*, 152–164, doi:10.1016/j.epsl.2014.11.031.
Toggweiler, J. R., and D. W. Lea (2010), Temperature differences between the hemispheres and ice age climate variability, *Paleoceanography*, *25*, PA2212, doi:10.1029/2009PA001758.
Ujiié, H., and Y. Ujiié (1999), Late Quaternary course changes of the Kuroshio current in the Ryukyu Arc region, northwestern Pacific Ocean, *Mar. Micropaleontol.*, *37*, 23–40.
Ujiié, Y., and H. Ujiié (2000), Distribution and oceanographic relationships of modern planktonic foraminifera in the Ryukyu Arc region, Northwest Pacific Ocean, *J. Foraminiferal Res.*, *30*, 336–360, doi:10.2113/0300336.
Ujiié, Y., and H. Ujiié (2006), The changes of surface and intermediate waters for the last 250 ka in the Okinawa Trough and south off Ishigaki Island [in Japanese with English abstract], *Kaseki*, *79*, 43–59.
Ujiié, Y., H. Ujiié, A. Taira, T. Nakamura, and K. Oguri (2003), Spatial and temporal variability of surface water in the Kuroshio source region, Pacific Ocean, over the past 21,000 years: Evidence from planktonic foraminifera, *Mar. Micropaleontol.*, *49*, 335–364, doi:10.1016/S0377-8398(03)00062-8.

Vivier, F., K. A. Kelly, and L. Thompson (2002), Heat budget in the Kuroshio Extension Region: 1993-99, *J. Phys. Oceanogr.*, *32*, 3436–3454, doi:10.1175/1520-0485(2002)032<3436:HBITKE>2.0.CO;2.

Wilke, I., T. Bickert, and F. J. C. Peeters (2006), The influence of seawater carbonate ion concentration [CO_3^{2-}] on the stable carbon isotope composition of the planktic foraminifera species *Globorotalia inflata*, *Mar. Micropaleontol.*, *58*, 243–258, doi:10.1016/j.marmicro.2005.11.005.

William, T. C., F. L. Parker, and W. H. Berger (1980), Faunal and solution patterns of planktonic foraminifera in surface sediments of the North Pacific, *Mar. Micropaleontol.*, *5*, 329–399, doi:10.1016/0377-8398(80)90019-5.

Xu, X., and M. Oda (1999), Surface-water evolution of the eastern East China Sea during the last 36,000 years, *Mar. Geol.*, *156*, 285–304, doi:10.1016/S0025-3227(98)00183-2.

Yamasaki, M., and M. Oda (2003), Sedimentation of planktonic foraminifera in the East China Sea: Evidence from a sediment trap experiment, *Mar. Micropaleontol.*, *49*, 3–20, doi:10.1016/S0377-8398(03)00024-0.

Yasuda, T., and K. Hanawa (1999), Composite analysis of North Pacific subtropical mode water properties with respect to the strength of the wintertime East Asian monsoon, *J. Oceanogr.*, *55*, 531–541, doi:10.1023/A:1007843525069.

Yasuda, T., and Y. Kitamura (2003), Long-term variability of North Pacific Subtropical Mode Water in response to spin-up of the subtropical gyre, *J. Oceanogr.*, *59*, 279–290, doi:10.1023/A:1025507725222.

You, Y. (2003), The pathway and circulation of North Pacific Intermediate Water, *Geophys. Res. Lett.*, *30*(24), 2291, doi:10.1029/2003GL018561.